We are IntechOpen,
the world's leading publisher of
Open Access books
Built by scientists, for scientists

6,900
Open access books available

185,000
International authors and editors

200M
Downloads

Our authors are among the

154
Countries delivered to

TOP 1%
most cited scientists

12.2%
Contributors from top 500 universities

CLARIVATE ANALYTICS
BOOK CITATION INDEX
INDEXED

WEB OF SCIENCE™

Selection of our books indexed in the Book Citation Index
in Web of Science™ Core Collection (BKCI)

Interested in publishing with us?
Contact book.department@intechopen.com

Numbers displayed above are based on latest data collected.
For more information visit www.intechopen.com

Advanced Sintering Techniques in Design of Planar IT SOFC and Supported Oxygen Separation Membranes

Vladislav Sadykov et al.[*]
Boreskov Institute of Catalysis, Novosibirsk State University, Novosibirsk,
Russia

1. Introduction

Thin film solid oxide fuel cells (SOFC) operating in the intermediate temperature (IT) range are now considered as promising for distributed, mobile, standby or auxiliary power generation. At present one of the most important scientific aims in design of solid oxide fuel cells is to lower the operating temperatures to 600-800°C. In this temperature range, majority of problems inherent to SOFC operating at high (950-1000°C) are alleviated. Thus, cations interdiffusion and solid state reactions between electrolyte and electrodes are hampered and thermal stresses are decreased which prevent degradation of the functional layers [Yamamoto, 2004]. Hence, design of thin film SOFC requires also elaboration of nano-structured electrodes compatible with electrolytes from chemical and thermophysical points of view and providing a developed three-phase boundary (TPB). In this respect, broad options are provided by design of nanocomposite mixed ionic-electronic conducting (MIEC) functional layers – (Sadykov et al., 2010; Sadykov et al., 2009; Sadykov et al., 2008).

One of the most demanding problem in solid oxide fuel cells design is caused by the necessity of co-sintering of thin layers (electrolyte, functionally graded nanocomposite cathode) to provide required density without degradation of their transport, electrochemical and thermo-mechanical properties. The most developed and cost-effective are methods based upon supporting electrolyte powders with addition of organic binders and dispersants via screen-printing (Souza et al., 1998), tape casting (Kobayashi et al., 2002) or slurry coating technique (Jung et al., 2007). Thus supported «green» layers are sintered at

[*] Vladimir Usoltsev[1], Yulia Fedorova[1], Natalia Mezentseva[1], Tamara Krieger[1], Nikita Eremeev[1], Marina Arapova[1], Arcady Ishchenko[1], Alexey Salanov[1], Vitaly Pelipenko[1], Vitaly Muzykantov[1], Artem Ulikhin[2], Nikolai Uvarov[2], Oleg Bobrenok[3], Alexander Vlasov[4], Mikhail Korobeynikov[4], Aleksei Bryazgin[4], Andrei Arzhannikov[4], Petr Kalinin[4], Oleg Smorygo[5] and Manfred Thumm[6]
[1]Boreskov Institute of Catalysis, Novosibirsk State University, Novosibirsk, Russia
[2]Institute of Solid State Chemistry and Mechanochemistry, Novosibirsk, Russia
[3]Institute of Thermal Physics, Novosibirsk, Russia
[4]Budker Institute of Nuclear Physics, Novosibirsk, Russia
[5]Institute of Powder Metallurgy, Minsk, Belarus
[6]Karlsruhe Inst. Technology, Karlsruhe, Germany

temperatures ~ 1400°C. As a rule, high sintering temperatures required for electrolyte densification impose restrictions on the nature of electrode materials. Thus, at temperatures of sintering exceeding 1200°C, application of cathode substrates comprised of Sr-substituted perovskites could result in formation of isolating La(Sr)-zirconate layers (Chiba et al., 2008). Similarly, in the case of metal substrates high-temperature sintering is possible only in vacuum or in reducing gas atmospheres (Tucker, 2010). Another approach to supporting thin layers of electrolytes is based upon application of vapor deposition methods operating at substrate temperatures below 1000°C. This prevents formation of undesired phases in the course of synthesis, thus broadening the scope of electrode materials which can be used as electrolyte substrates. Among these methods, the most developed are different versions of Chemical Vapor Deposition (CVD) and Plasma Deposition (either in air or in vacuum) (Yamane & Hirai, 1987; Schiller et al., 2000; Minh, 1993).

Traditional sintering approaches requiring too high temperatures often failed in this respect. In design of supported oxygen-separation membranes, similar problems appear due to necessity of sintering thin dense mixed ionic-electronic conducting nanocomposite layers supported on macroporous ceramic (cermet or metal) substrates. For example to get Gd-doped ceria (GDC) pellet with density 97% from agglomerated commercial powders by simple heating in the furnace, required temperature is 1600-1700°C (Ma et al., 2004). Densification rate of GDC powder was found to increase only after 1100°C being accompanied by grain growth (Zhang & Ma, 2004). By using weakly agglomerated GDC nanopowders (average grain size 10 nm), the density of 94% from the theoretical value was achieved after sintering at 1100°C for several hours, and after 108 hours the relative density increased up to 99%. Increasing sintering temperature to 1200-1300°C allows to obtain 97-99 % density samples after 5 hours dwelling (Ivanov et al., 2007). Sintering of composites of ceria with strontium-doped lanthanum manganites was also studied using conventional techniques. Samples with 95-98% density could be obtained at temperatures 1350-1400°C. Sintering dynamics was found to depend upon samples composition, the best sinterability being observed for samples containing 30-70% ceria (Cutler et al., 2003). Together with application of nanosized powders, a popular approach in conventional sintering aiming at lowering sintering temperature is based upon using special sintering additives. Some of these additives form melts which enhance mass transfer between the particles of materials with a higher melting point. Bismuth oxide melts at 820°C and can substitute rare earth cations in the functional layers improving electrochemical performance. Sintering of GDC was enhanced by adding small amounts of Bi_2O_3: samples of GDC containing 1 wt% bismuth sintered at 1200-1400°C for 2 - 4 h were dense bodies (98-99% of theoretical density) which is achieved at temperatures lower by 250-300°C than required for sintering of undoped GDC (Gil at al., 2007). Moreover, even refractory additives can improve sintering via affecting defect chemistry at interfaces. Thus, the density and grain size of sintered Gd-doped CeO_2 increased with adding up to 2 mol. % Al_2O_3 while decreasing at a higher content of this additive (Lee et al., 2004 ; Liu at al., 2008). Similarly, iron oxide addition via mechanical activation treatment also provides a higher density of GDC (Zhang at al., 2004). The maximum density was obtained by adding 5 mol.% Ga_2O_3 to GDC at sintering temperature 1400°C (Lee et al., 2004). Combination of nanosized freeze-dried powders with addition of 1-3 mol.% cobalt to GDC allowed to get 94% density at 1000° C [Perez-Coll et al., 2003].

For sintering of cathode or membrane perovskite layers, silver or Ag-Pd alloy aids were successfully used (Chen et al, 1992).

Advanced sintering techniques are based upon application of high-energy irradiation that could be focused directly on the sample or even functional layer (as described in selective laser sintering studies (Kumar, 2003). Electron beams as PVD modification were used for deposition of alumina or composite cermets functional layers of carbides/nitrides (Singh & Wolfe, 2005). Only a few works mention e-beam as a promising approach to deposit thin and dense YSZ or GDC electrolyte layer on electrode (mainly NiO/YSZ anode) (Laukaitis et al., 2007; Lemkey et al., 2005). Deposition through the vapor (PVD or CVD) ensures thin uniform layers but, unfortunately, this approach requires high vacuum that increases costs and reduces commercial usage. Nevertheless, e-beam technique was used for direct sintering, including application of high-energy e-beams to produce layered metal composites (Zaeh&Kahnert, 2009), sintering of zirconia and zirconia-corundum composites etc. (Annenkov, 1996). Enhanced sintering of ceramics under e-beams action is explained by dissipation of radiation energy in heterogeneous structures, thermal-diffusion stimulation of mass transfer due to point defect formation and increase of thermal vibrations of the lattice (Annenkov, 1996)

Compared with radiation-induced sintering techniques, microwave heating at frequency 2.45 GHz is more broadly applied for sintering of zirconia-based electroceramics (Alexeff & Meek, 2011; Mazaheri et al., 2008). Zirconia or ceria- based materials have a low microwave absorption at temperatures below 400°C (Jiao, 2011). Jump-like change of their dielectric properties at 400-1000°C requires to use special susceptors with a better absorption for preheating samples and smoothing the heating curve. As a susceptor usually disks of SiC were used to provide so called hybrid microwave sintering. Microwave heating produces samples sintered to density 90-95% of the theoretical value at temperatures lower by 200°C than conventional heating (Mazaheri et al., 2008 ; Charmond et al., 2010). However, the maximum density obtained for doped zirconia samples in these conditions was ca 98%, and to produce fully dense samples the hybrid mode heating was used with dwelling about 1 hour at 1350°C (Charmond et al., 2010). Microwave heating uses also significantly higher heating rates 5-50° (and even 200°)/min as compared with conventional sintering carried out at a heating rate 2-5°/min with dwelling at the maximum temperature for 5-10 hours. This becomes possible due to very uniform heating without space gradients of temperature in the sample. A higher heating rate provides a lower average grain size (2.3 µm at 5°/min vs 0.9 µm at 50o/min) (Mazaheri et al., 2008 ; Charmond et al., 2010). Despite all these apparent advantages, up to date these advanced techniques have not been systematically applied for sintering functional layers comprised of mixed ionic –electronic conductors –perovskites and their nanocomposites with different electrolytes as required in design of thin film IT SOFC and oxygen separation membranes.

This work presents results of research aimed at filling such a gap and providing verification of these advanced sintering techniques (e-beam and microwave heating) for such an application. Functional layers were comprised of oxides with ionic conductivity (doped ceria, doped zirconia and δ-Bi_2O_3, doped La silicate with apatite structure) and mixed ionic-electronic conductivity (perovskites and their nanocomposites with electrolytes). Effect of sintering parameters on the real structure/microstructure and functional properties of these

materials was elucidated. Experimental samples of button-size fuel cells and oxygen separation membranes were manufactured using advanced sintering techniques and successfully tested showing promising performance.

2. Experimental

2.1 Powder synthesis

Nanocrystalline complex oxides with ionic conductivity (fluorite-type electrolytes GDC, YSZ, δ-Bi_2O_3 stabilized by Er or Y+Sm) and mixed ionic-electronic conductivity (rare-earth manganites, nickelates, ferrites, cobaltites and their solid solutions including those doped by Sr and/or Bi) were synthesized by modified polymerized polyester citric acid-ethylene glycol precursors (Pechini) and mechanical activation routes. Synthesis procedures and structural features of these complex oxides are described in details elsewhere (Kharlamova et al., 2011; Sadykov et al., 2011). Nanocomposites were prepared by ultrasonic dispersion of the mixture of powders in isopropanol (solvent) using a T25 ULTRA-TURRAX (IKA, Germany) homogenizer with addition of polyvinyl butyral. Detailed compositions of complex oxide and their composites prepared for sintering are summarized in Table 1.

Materials	Abbreviation	Chemical composition	Geometry	Sintering techniques*
Cathode	LFN	$LaFe_{0.7}Ni_{0.3}O_{3-\delta}$	Pellets	CH
	LFC	$LaFe_{0.5}Co_{0.5}O_{3-\delta}$	Pellets	CH
Cathode composite	LFN-GDC	$LaFe_{0.7}Ni_{0.3}O_{3-\delta}$ (50 wt.%)-$Ce_{0.9}Gd_{0.1}O_{2-\delta}$ (50 wt.%)	Pellets	CH, RTS
	LFC-GDC	$LaFe_{0.5}Co_{0.5}O_{3-\delta}$ (50 wt.%)-$Ce_{0.9}Gd_{0.1}O_{2-\delta}$ (50 wt.%)	Pellets	CH, RTS
Electrolyte	GDC	$Ce_{0.9}Gd_{0.1}O_{2-\delta}$	Pellets Layer	CH, RTS, MH
	YSZ	$Y_{0.08}Zr_{0.92}O_{2-\delta}$	Pellets	MH
	BE	$Bi_{0.5}Er_{0.5}O_{2-\delta}$	Pellets	CH
	BYS	$Bi_{1.5}Y_{0.3}Sm_{0.2}O_{2-\delta}$	Pellets	CH, MH
Anode	NiO/YSZ	NiO (60%)-$Y_{0.16}Zr_{0.84}O_{2-\delta}$ (40%)	Pellets, Foam-based	CH, RTS CH

* CH- conventional heating, MH- microwave heating, RTS-radiation-thermal sintering

Table 1. Compositions and samples geometry.

2.2 Samples preparation for sintering

Pellets were uniaxially pressed from powders under 5.5 t/cm². As a porous metal substrate for composite anode or cathode, a unique type of macroporous planar Ni-Al foam substrate with a high electric and thermal conductivity, thermal stability and corrosion resistance was used (Smorygo et al., 2008; Sadykov et al. 2010). Along with these metal substrates, traditional NiO/YSZ planar anode substrates covered by thin layers of YSZ electrolyte were used for supporting cathode layers (Sadykov et al, 2009, 2011). Functional layers were supported by slip casting or screen-printing on the support surface.

2.3 Sintering techniques

Functional layers and uniaxially pressed pellets were sintered by different techniques: conventional heating (CH) in the furnace at temperatures up to 1300°C (nanocomposites) or 1400°C (electrolytes) with or without sintering aids (Bi or Ag nitrates, etc) in different gas atmospheres (air, Ar, etc); microwave heating (MH) or radiation-thermal sintering (RTS) under electron beam action.

For conventional heating, a high-temperature oven equipped with a quartz reactor specially designed for heating in the argon flow was used.

MH was carried out using a system based on gyrotron with frequency 24 GHz specially designed for heating of materials. Samples were heated by the focused radiation (power 0.5-1.5 kW) up to 1000-1200°C with heating rate 50°/min followed by dwelling at the final temperature for 30 min and then cooling to room temperature.

RTS was carried out on an ILU-6 accelerator that gives electron pulses with a high (2.4 MeV) energy. Temperature was varied in range of 900-1200 °C (heating rate 30-40 °/min) by changing the frequency in the range of 8-20 Hz. Time of treatment was varied in the range of 10-240 min.

2.4 Characterization of the real structure and functional properties

Genesis of the real structure of sintered functional layers and pellets was studied in details by X-ray powder diffraction, high resolution transmission electron microscopy and scanning electron microscopy with local elemental analysis by EDX. XRD patterns were obtained with an ARLX'TRA diffractometer (Thermo, Switzerland) using CuK$_\alpha$ monochromatic radiation (λ=1.5418 Å) in 2θ range 5-90°. Transmission Electron Microscopy (TEM) micrographs were obtained with a JEM-2010 instrument (lattice resolution 1.4 Å, acceleration voltage 200 kV). Analysis of the local elemental composition was carried out by using an energy-dispersive EDX spectrometer equipped with Si(Li) detector (energy resolution 130 eV).

Transport properties were characterized by impedance spectroscopy and oxygen isotope heteroexchange. Conductivity was measured in air with a MO-10 Micro-Ohmmeter at 25 Hz frequency with four Ag paste electrodes placed symmetrically at a perimeter of the pellet. The oxygen mobility was characterized by the temperature -programmed oxygen isotope exchange (a static installation with MS control of the gas phase isotope composition at pO$_2$ 4 Torr). Performance of functional layers sintered by using different techniques was tested using respective devices: button-size fuel cells operating with wet H$_2$–air feeds and reactors equipped with supported membranes operating in the mode of oxygen separation from air into He stream (Sadykov et al, 2010, 2011).

3. Results and discussion

3.1 Effect of sintering stage on the real structure of SOFC materials

Electrolytes

Fresh (after synthesis) powders of GDC and BE are characterized by cubic fluorite –like structure, with some tetragonal distortions for YSZ. After sintering stage (radiation-thermal

treatment, microwave or conventional heating) new phases were not revealed and no significant changes in diffraction pattern could be observed (Fig. 1). For fresh BYS sample, diffraction pattern corresponds to rhombohedral $Bi_{0.775}Sm_{0.225}O_{1.5}$ phase [89-4391, 44-0043] (Fig. 2). After sintering, it transforms into cubic fluorite phase of $Bi_{1.5}Y_{0.5}O_3$ type [33-0223] with lattice parameter a =5.511 Å (CH) - 5.507 Å (RTS). The lattice parameters of GDC and YSZ calculated for fresh or sintered samples vary only slightly (for 1-2%). Diffraction peaks are narrowed after sintering reflecting grain growth. Thus, X-ray particle sizes calculated by using the Scherrer equation change from 10.8 nm for fresh YSZ sample to 59.8 nm after radiation treatment. For BYS, variation is smaller –from 66.0 nm for fresh sample to 80 nm for sample after RTS.
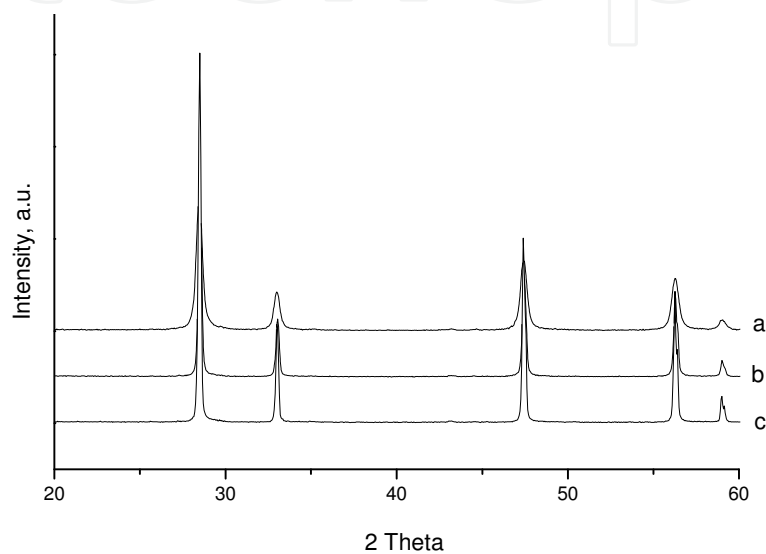
Fig. 1. Effect of sintering on XRD patterns of GDC electrolyte fresh (a), after microwave heating (b) and after radiation-thermal treatment (c).
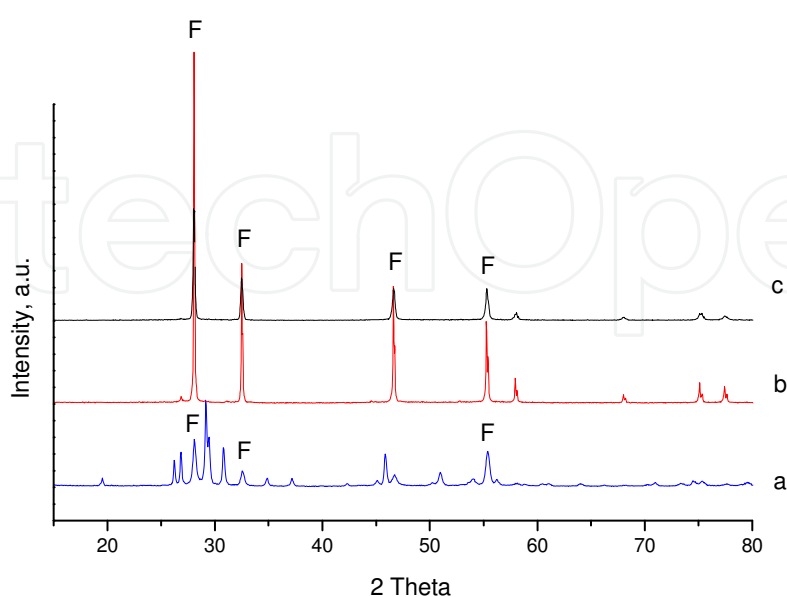
Fig. 2. Effect of sintering on XRD patterns of BYS electrolyte fresh (a), after conventional heating (b) or microwave heating (c).

Fig. 3 presents high resolution TEM images of GDC sample -fresh and after RTS or MH. Fresh sample consists of disorderly stacked nanosized (10-20 nm) domains. Sintering increases domains size up to 50-100 nm and provides their coherent stacking. EDX analysis revealed that the chemical composition of domains in sintered oxide is close to that in fresh sample $Ce_{0.86-0.91}Gd_{0.14-0.09}$. Similar variation of particle size and the mode of stacking after radiation-thermal treatment was observed by TEM for YSZ powder

TEM images for BYS electrolyte are presented in Fig. 4. The 111 lattice spacing observed (3.172 Å) is close to that in $Bi_{1.5}Y_{0.5}O_3$ (PDF#33-223 (Fm3m). The chemical composition of fresh sample at particles edges is characterizes by a higher bismuth content ($Bi_1Y_{0.9}Sm_{0.6}$) as compared with the core ($Bi_{0.4}Y_1Sm_{0.3}$). This segregation disappears after sintering being accompanied by rotational disordering of nanosized domains stacking. Hence, cooperative rhombohedral distortion of fluorite-like BYS structure in fresh sample can be caused by spatial nonuniformity of dopants distribution in particles.

a

b

c
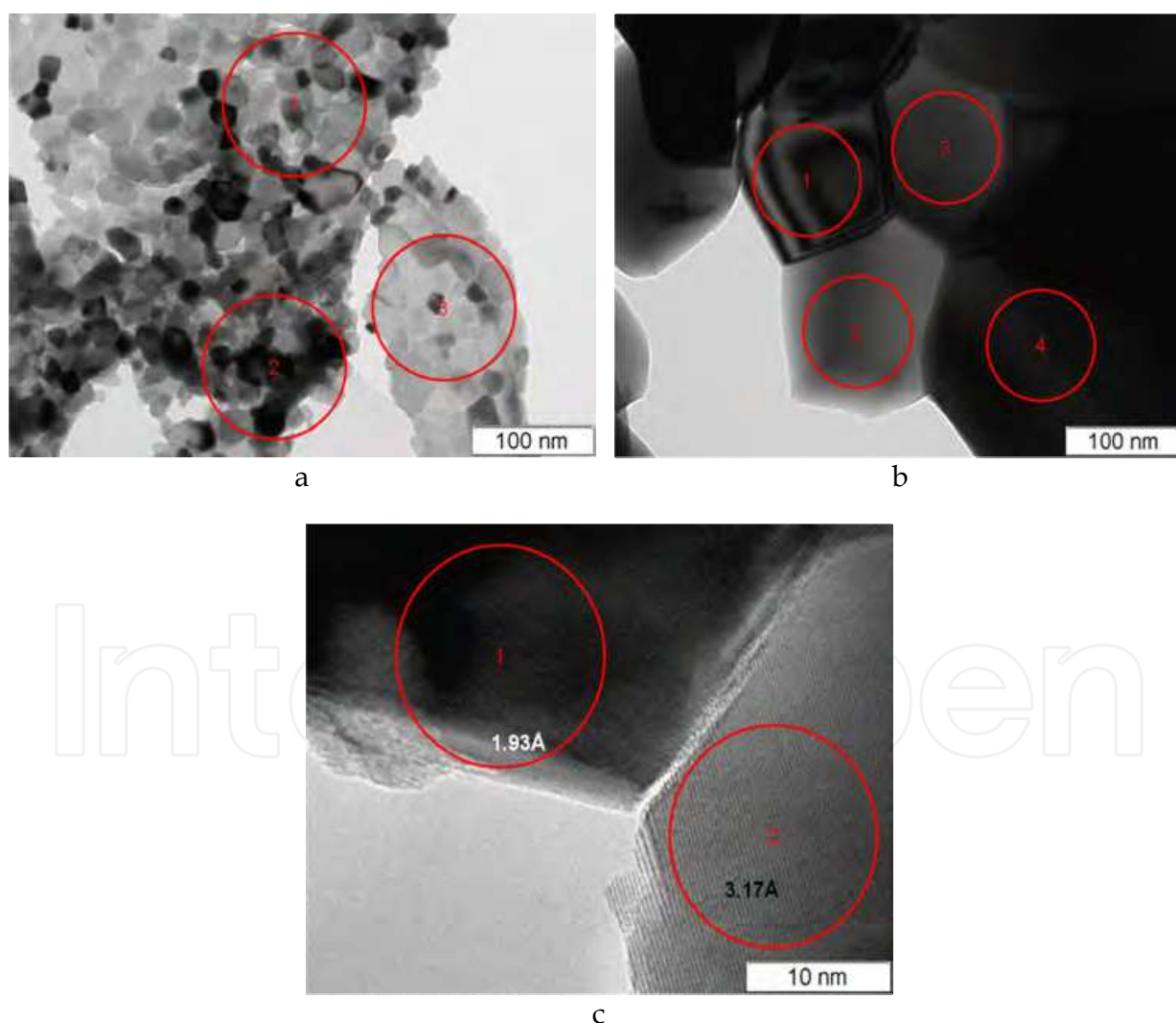
Fig. 3. TEM images of GDC after synthesis (a), radiation-thermal sintering at 1200 ˚C
(b) or microwave heating at 1200˚C (c).
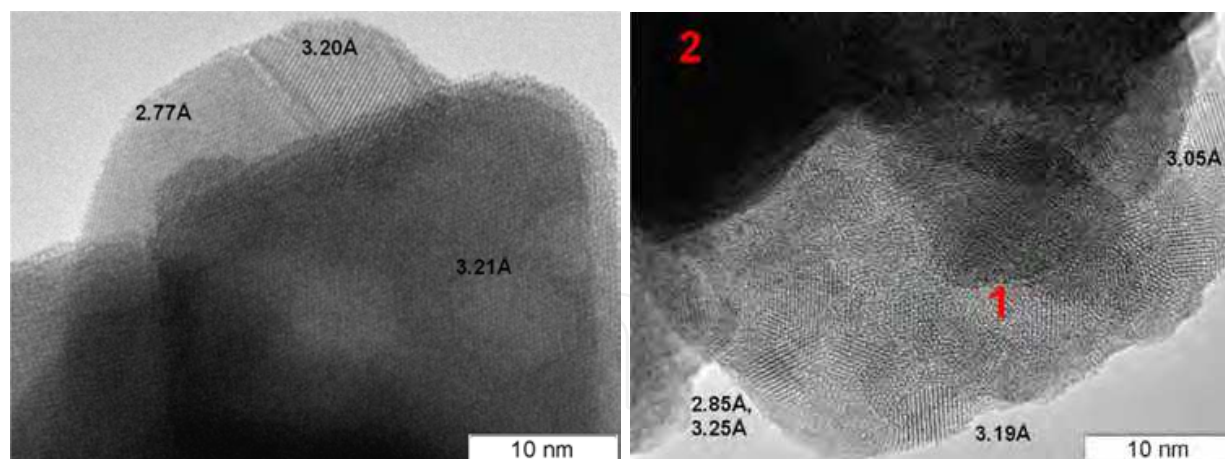
Fig. 4. TEM images of BYS after synthesis (a) and microwave heating at 900˚C (b).

Hence, advanced sintering procedures resulted in substantial grain growth even for rather refractory electrolytes (GDC, YSZ) at moderate temperatures.

Cathode nanocomposite materials

After synthesis, complex perovskite oxides LFN and LFC (P) have the rhombohedral –type structure (space group R3-c) , and GDC - fluorite-type (F) cubic structure. The same structures are observed after sintering by conventional heating as well as by radiation treatment (Fig. 5). Some shift of reflections is observed after sintering due to redistribution of cations between P and F phases (Sadykov , 2010). X-ray particle sizes of both phases in composites increase with the temperature of sintering. Thus, for perovskite phases, after radiation-thermal sintering of composites at 1100˚C, X-ray particle sizes increase from 20-30 nm for fresh samples to 90-100 nm. Variation of more refractory GDC phase particle size is less pronounced -from 10-20 nm to ~ 40-50 nm.
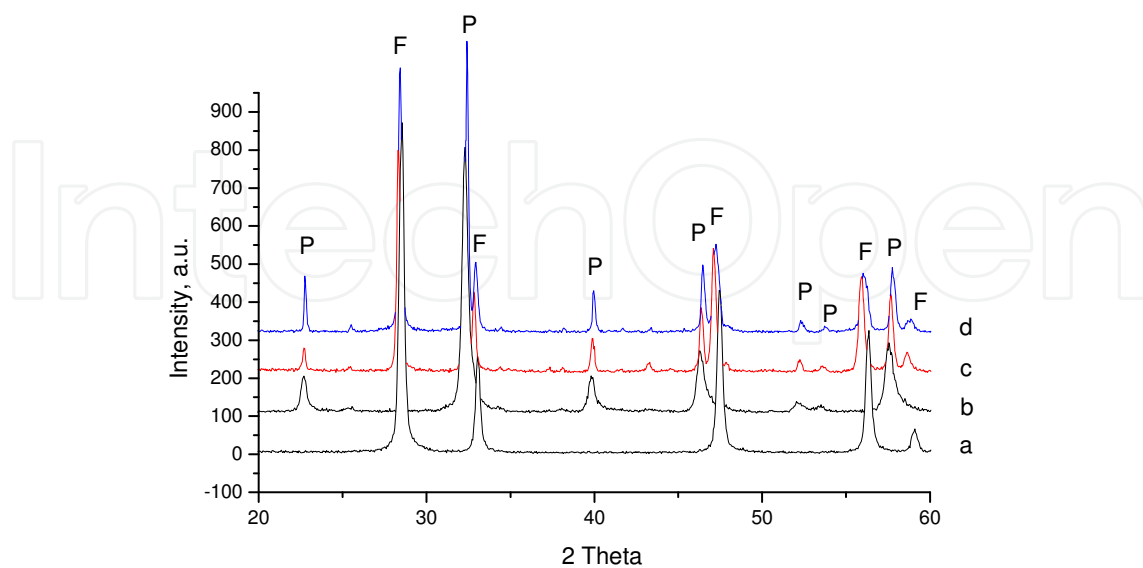
Fig. 5. Effect of sintering on XRD patterns of LFN-GDC composite (a-GDC fresh, b-LFN fresh, c- LFN-GDC after CH 1300˚C, d - LFN-GDC, after RTS). P – perovskite-type phase, F – fluorite-type phase.

Fig 6. presents high- resolution TEM images for LFN-GDC cathode composite after radiation-thermal treatment. As judged by TEM data, reasonably uniform spatial distribution of perovskite and fluorite domains is observed. As follows from EDX data, pronounced redistribution of elements between P and F domains takes place. La and Fe from perovskite phase move to fluorite-type oxide while cerium and gadolinium ions migrate to perovskite structure. Nickel has not demonstrated significant mobility. Domain boundaries appear to be rather coherent providing a good epitaxy between P and F phases. Typical domain size for both samples is about 10-50 nm.
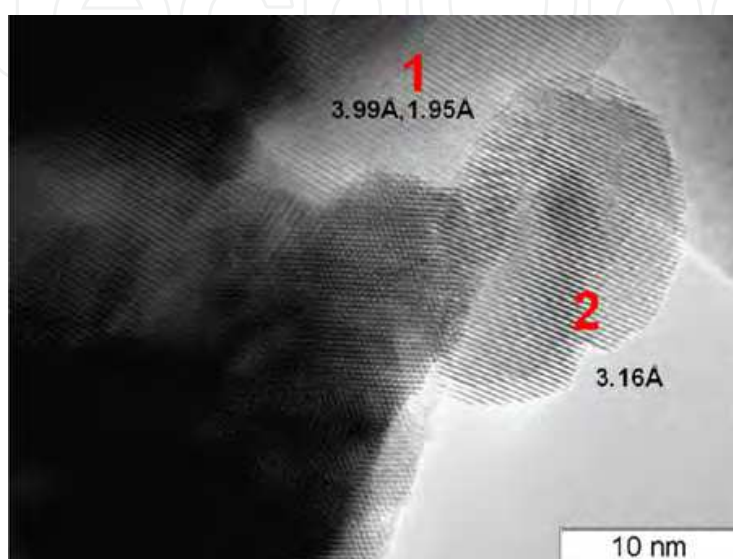
Fig. 6. TEM images of LFN-GDC composite after RTS at 1100° C. 1- LFC domain, 2- GDC domain.

3.2 Microstructure of sintered SOFC materials

Solid electrolytes (GDC, BE)

Microstructure of sintered pellets of solid electrolytes was studied by SEM. Figs. 7. and 8 present typical microstructure of samples after radiation-thermal treatment and microwave heating. Both electrolytes demonstrate a high density without visible cracks. Some closed porosity in observed in BYS (Fig. 8).

The average grain size of GDC oxide after RTS (0.2-0.5 µm) seems bigger than domains of GDC sintered by microwave heating (0.1-0.4 µm). This fact can be explained by very fast diffusion in the solid under e-beam. Thus, microwave heating stimulates local radiation absorption, and only part of this energy dissipates into heat that stimulates grain growth. Moreover, RTS was held for 150 min vs 90 min of MH. For conventional sintering it is a common knowledge that increasing sintering time increases grain size.

Cathode materials (LFN-GDC, LFC-GDC)

Sintering of bulk cathode composites was studied using radiation-thermal sintering and conventional heating techniques. In Figs. 9 and 10 values of density estimated by Archimedes method are presented in dependence on sintering temperature and duration of radiation treatment.
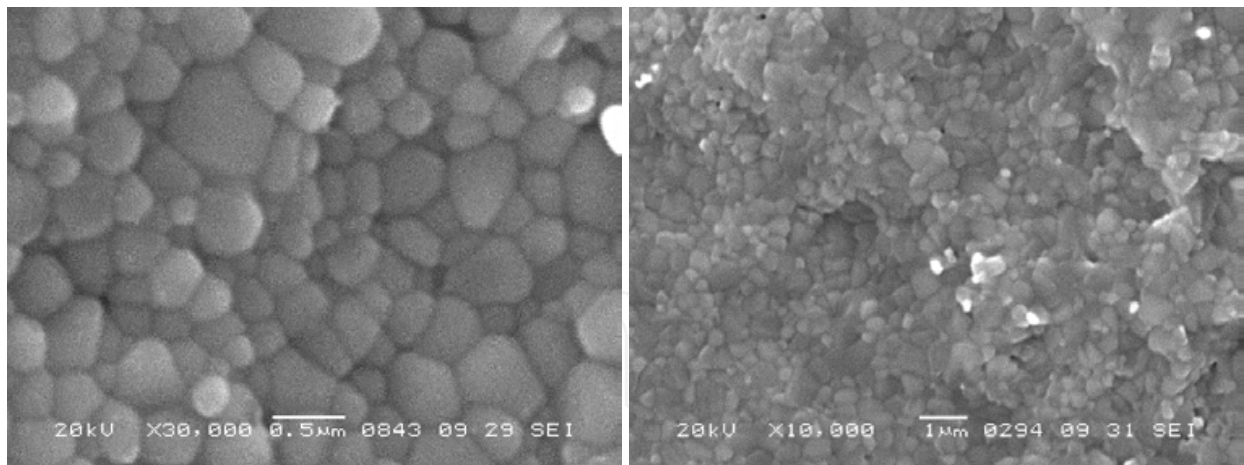
Fig. 7. SEM images demonstrating bulk (cross-section) structure of GDC after radiation-thermal sintering (a) and after microwave heating (b).
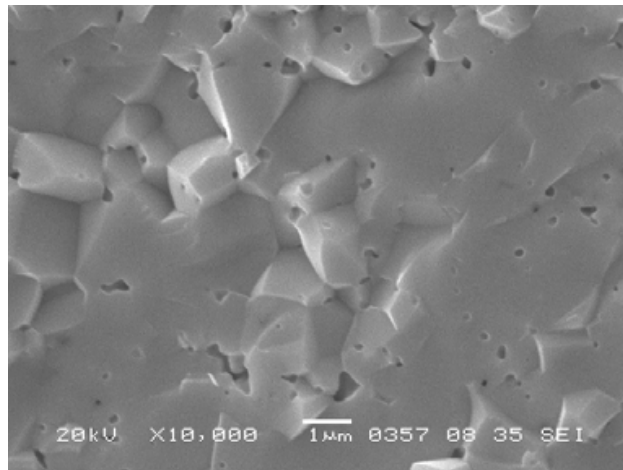

Fig. 8. SEM image demonstrating internal structure of BYS after microwave heating at 900˚C.
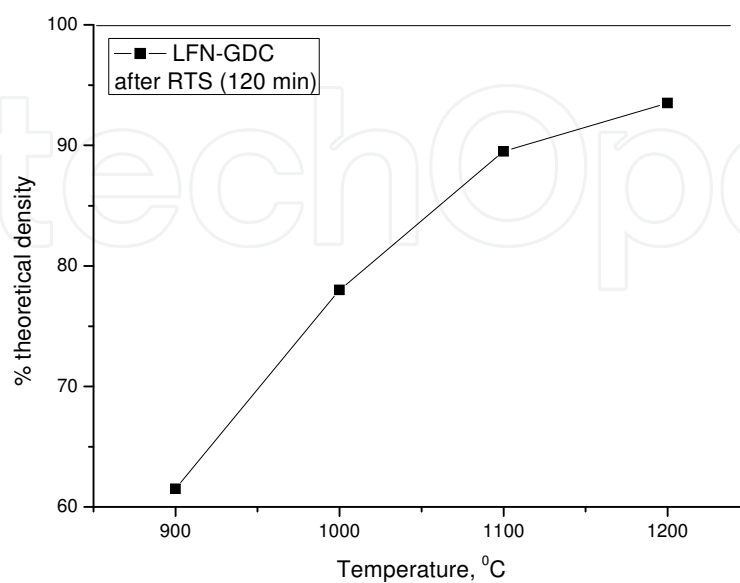

Fig. 9. Influence of temperature on density of LFN-GDC cathode composite.

As follow from Fig.10, duration of radiation-thermal treatment has a small effect on the real density of sample. In fact, after 60 min of RTS no significant increase of density was observed. On the contrary, the temperature strongly affects the density increasing it from 60% at 900˚C to 95% at 1200˚C.
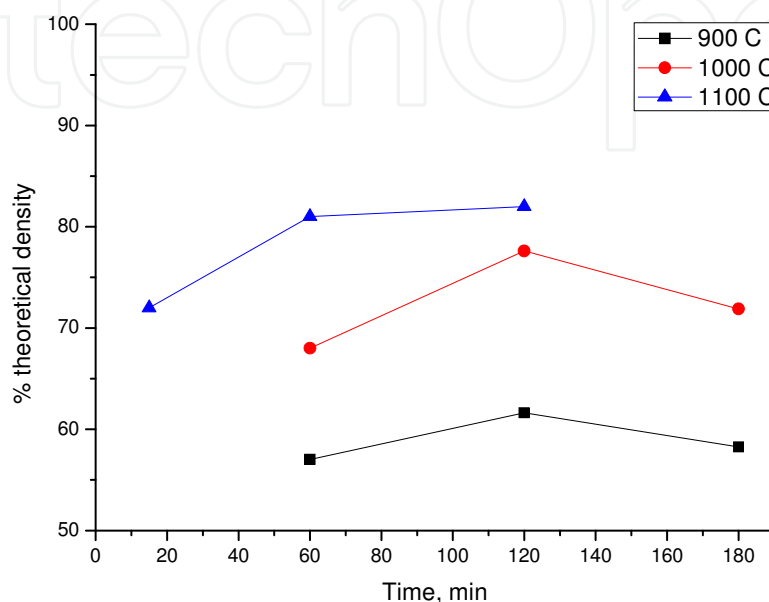
Fig. 10. Effect of sintering time on the density of cathode LFN-GDC composite.

It is worth noting that all samples sintered by RTS have a high mechanical strength even after RTS at 900˚C. This fact is obviously explained by formation of crystal-type contacts in the bulk of composite. Nothing of this kind was observed by conventional sintering at the same temperatures and sintering time. Another important fact consists in the level of theoretical density: by using RTS technique we obtained 95 % of theoretical density at 1200˚C and 60 min treatment, while by conventional sintering it can be achieved only after keeping at 1300˚C for 5 hours.

The internal microstructure of sintered cathodic composite was studied by SEM images of cross-sections in back-scattered electrons (Fig. 11). Dark regions in this image correspond to perovskite-type phase, and gray to GDC. After sintering, interpenetrating structures of perovskite phase (electronic conductor) and fluorite-type GDC (ionic conductor) are observed. LFN-GDC sintered by conventional heating is characterizes by residual porosity (typical size of pores 0.5-1 μm) due to shrinkage of nanosized particles. The same features of microstructure were observed for LFC-GDC composite. Hence, cathodic composites based on lanthanum ferrites/cobaltite with GDC are expected to demonstrate the same features during radiation-thermal sintering: fast shrinkage under e-beam, formation of matrix even at moderate temperatures, which prevents diffusion of La cations into electrolyte typical to high-temperature treatments.
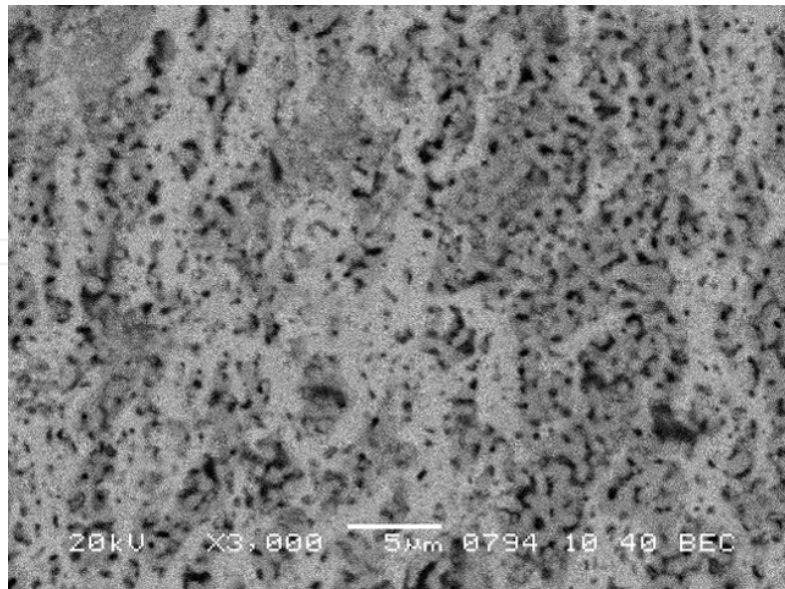
Fig. 11. Internal microstructure by SEM images in back-scattered electrons of LFN-GDC nanocomposite, CH 1300˚ C.

3.3 Microstructure of functional layers on metallic anodic substrates

Typical SEM images of different electrolyte layers supported on anodic substrate NiO/YSZ/Ni-Al foam are shown in Fig. 12. GDC layer was sintered to complete density by radiation –thermal treatment at 1200˚C (Fig. 12a), which is ~ 200˚C lower than for conventional sintering. Bi-Er and BYS layer were sintered by this method to a similar density even at much lower (900˚C) temperature. Though small (less than 0.5 μm diameter) closed pores were observed, their share is estimated to be below 5%.

For Sr-doped lanthanum silicate electrolyte $La_9SrSi_6O_{26.5}$ known for its poor sinterability (Sadykov et al, 2010), porosity is apparently bigger (Fig. 12d), though the layer is also rather dense. Hence, for the latter type of electrolyte, combination of radiation-thermal treatment with sintering aids could be applied to provide complete layer densification.

Sintering of cathode composites should provide reasonably porous (porosity ~ 30-40%) mechanically strong layers strongly attached to the layer of electrolyte. As follows from Fig. 13a, radiation-thermal treatment (as well as microwave radiation) provides required characteristics combining porosity with developed triple-phase boundary to ensure both developed surface area for oxygen molecules activation and diffusion paths for oxygen ions to enter the electrolyte layer. At the same temperatures cathode layer sintered by conventional heating was only weakly attached to electrolyte.

On the other hand, for nanocomposite mixed ionic-electronic conducting layers supported on the surface of oxygen separation membrane, complete density/absence of porosity is required to provide selective oxygen permeation. As shown in Fig. 13b, Bi-containing composites are sintered to complete density by radiation-thermal treatment at moderate (900˚C) temperatures, thus meeting requirement.
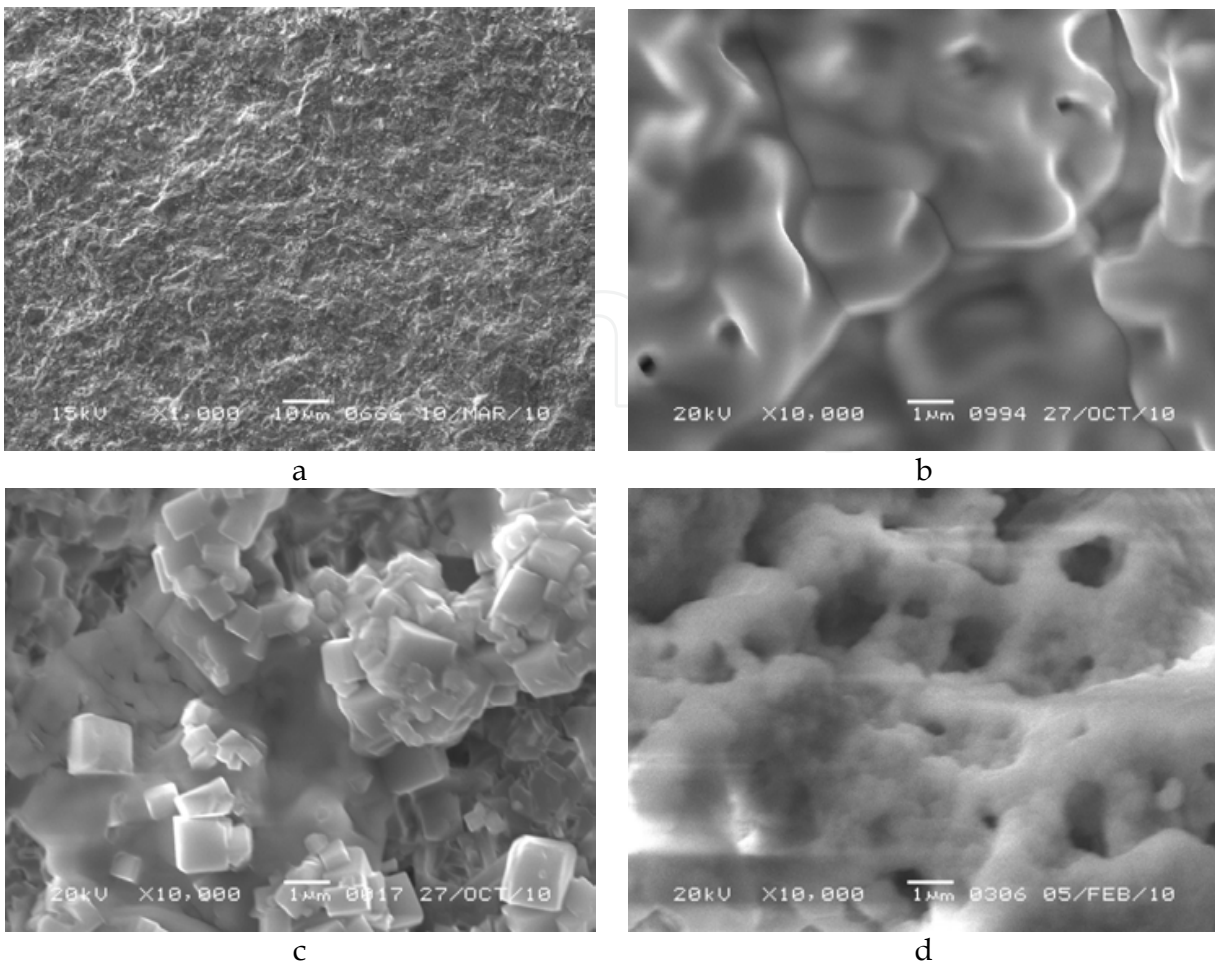
Fig. 12. SEM images of thin (10 microns) layers of electrolytes supported on anodic substrate NiO/YSZ/Ni-Al foam and sintered by radiation-thermal treatment at different temperatures. a- GDC, 1200˚C; b - BE , 900˚C, c-BYS, 900˚C, d- $La_9SrSi_6O_{26.5}$ with apatite structure, 1200˚C.
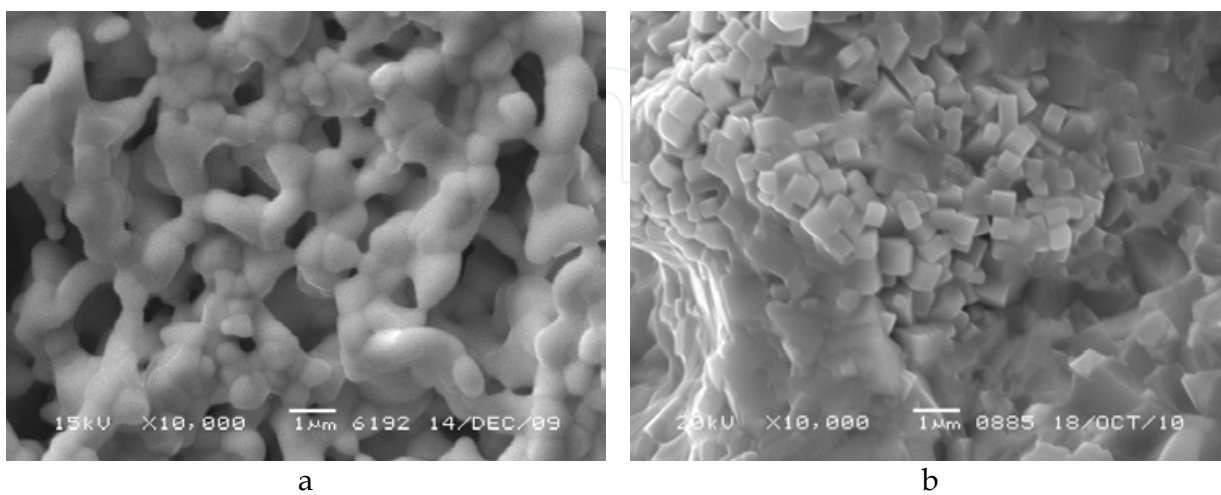

Fig. 13. SEM image demonstrating typical structure of LFN-GDC (a) and LaBiMn –BiEr layers (b) on Ni-Al foam-based substrates after radiation-thermal sintering at 900˚C.

3.4 Electrochemical and transport properties of cathode composite material

Conductivity

Fig. 14 demonstrates that conventional sintering provides a lower specific conductivity even at higher sintering temperature than RTS. While the main factor in controlling conductivity is certainly residual porosity of pellets, note that for the radiation-thermal treatment somewhat higher conductivity was observed after sintering at lower (900˚C) temperatures. This can be explained by a loss of oxygen from LFN at higher temperatures leading to conductivity decrease (Sadykov, 2011).
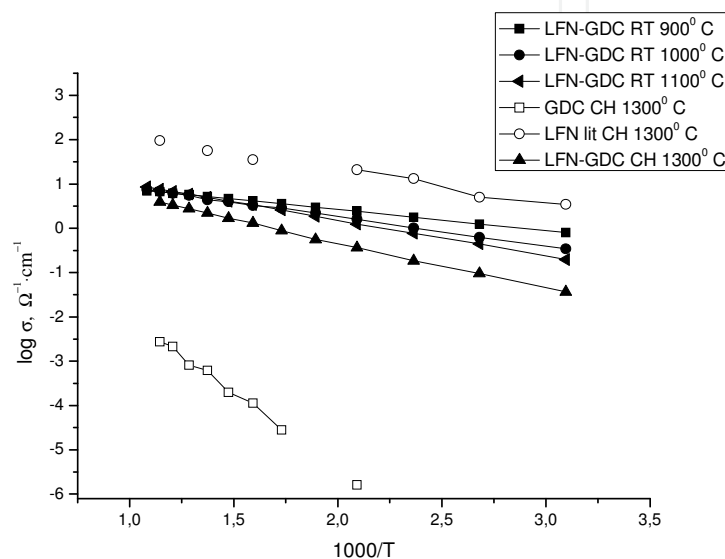
Fig. 14. Effect of sintering mode on specific conductivity of LFN-GDC samples after radiation-thermal sintering and conventional heating compared with literature data (Sadykov, Pavlova et al, 2010).

For LFC-GDC composite (Fig.15) sintering by e-beam at 1100˚C for 1 h provides the same level of specific conductivity as prolonged (5 hours) conventional sintering at 1300˚C. Surprisingly dwelling under e-beam for 2 hours or more has not improved conductivity. This can be explained by more pronounced interaction between phases in this nanocomposite as compared with LFN-GDC. Indeed, the difference between specific conductivity of LFC and LFC-GDC composite is ~ 3 order of magnitude, which is much bigger than that observed for LFN and LFN-GDC, respectively (Fig. 14).

Oxygen isotope heteroexchange

As a measure of oxygen mobility in perovskite-fluorite nanocomposites, so called dynamic extent of oxygen isotope exchange was shown to be simple and efficient characteristic varying in parallel with the oxygen diffusion coefficient (Sadykov et al, 2009-2010). It is defined as the number of oxygen atoms exchanged up to a given temperature in the temperature –programmed mode of heating the sample with the natural oxygen isotope

composition in a static reactor under contact with the gas phase containing initially only $^{18}O_2$. This value can be expressed either in oxygen monolayers (X_S) or as a fraction of all oxygen contained in the bulk of sample (X_V). Fig. 16 presents such dependence for LFN-GDC composites with different ratio of perovskite/fluorite phases. As follows from these results, for composites with a higher content of GDC, already at 700°C more than half of overall amount of bulk oxygen is exchanged, which is clearly possible only in the case of high oxygen mobility in the bulk of composite. The increase of oxygen mobility with the amount of GDC phase, and, hence, the length of perovskite-fluorite interface, agrees with suggestion that such an interface provides a path for fast diffusion due to its specific structure and composition (Sadykov et al, 2011). The values of X_v for LFN-GDC composites with a high GDC content are close to those for Sr-containing LSFC-GDC composites known for their very high oxygen mobility (Sadykov et al, 2008). Hence, even composites without Sr and Co in complex perovskites could provide a high bulk oxygen mobility combined with a low reactivity with respect to interaction with YSZ if their composition and sintering procedures are properly optimized.
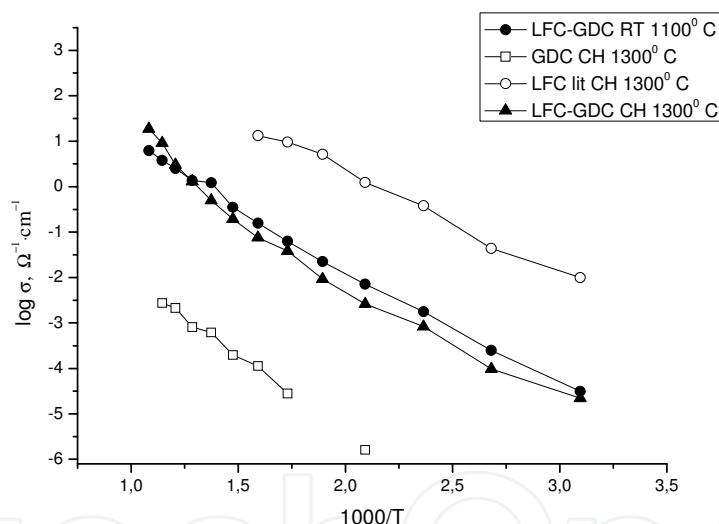

Fig. 15. Effect of sintering mode on specific conductivity of LFC-GD composite after radiation-thermal sintering and conventional heating compared with literature data (Sadykov, Pavlova et al, 2010).

3.5 Some characteristics of SOFC and oxygen separation membranes with co-sintered functional layers

3.5.1 Fuel cells

For assembling cells, a home-made Ni/yttria-doped zirconia (YSZ) anode substrate (the exposed cell surface area 1 cm^2) as well as Ni-Al foam supported NiO/YSZ layers with 10 micron thick 8YSZ layers supported by CVD were used. Cathode slurries made from

nano-powders ultrasonically dispersed in isopropanol with addition of butyral resin were deposited on half cells by air spray (perovskite + fluorite 10 microns thick nanocomposite functional layer, such as LSM-ScCeSZ or LSFN-GDC) and by painting (porous thick LSFN cathode layer) followed by drying and sintering at 900-1100˚C for 2 h using microwave or e-beam heating (Sadykov et al, 2011). The cell performance was evaluated using air at cathode side and humidified H_2 at anode side with Pt current collectors adding Pt or Ar pastes on the cathode side. For these cells, the typical level of power density at 700˚C was in the range of 500 mW/cm², which is promising for the practical application. Performance stability was demonstrated for short-term (~ 100 h) testing. No cracking or layers spallation was observed after testing. Decreased sintering temperature allowed to prevent any damages to anodic substrates during cells manufacturing as well as any undesired interaction between YSZ electrolyte and cathode layers leading to formation of isolating pyrochlore layers.
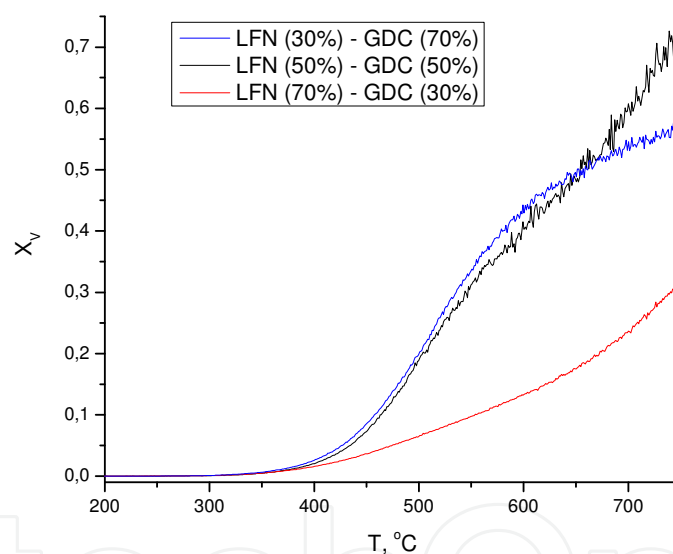

Fig. 16. Temperature dependence of the dynamic extent of exchange X_V for LFN-GDC composites sintered by microwave heating at 1100˚C. PO_2 = 4 Torr, heating ramp 5o/min.

3.5.2 Membrane performance

Fig. 17 presents the temperature dependence of oxygen flux through asymmetric supported oxygen separation membranes with Bi-containing perovskite-fluorite functional layers sintered by using microwave radiation (vide supra). As follows from these results, the values of oxygen flux are close to best results obtained with supported membranes in these conditions (Sadykov et al, 2010).
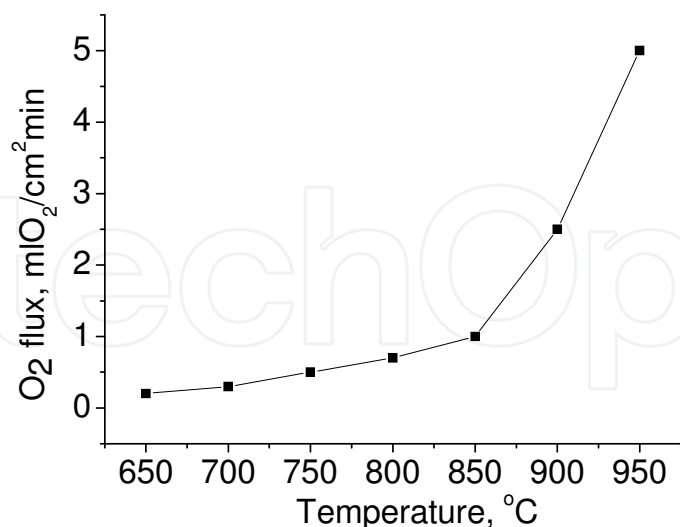
Fig. 17. Temperature dependence of oxygen flux under air/He gradient for supported asymmetric membrane comprised of La-BiMnO-YSmBi layers on binary Ni-Al foam substrate.

4. Conclusions

Advanced sintering techniques based upon radiation-thermal sintering by e-beam action and microwave heating allow to provide required density and consolidation of thin functional layers in design of intermediate temperature solid oxide fuel cells and oxygen separation membranes. Due to decreased temperature and duration of sintering as compared with conventional sintering methods, such negative phenomena as variation of functional layers phase composition, their cracking and damage of metallic substrates were prevented. For oxide mixed ionic-electronic conducting composites advanced sintering provides developed interfaces which act as paths for fast oxygen diffusion required for considered applications. As the results, fuel cells and oxygen separation membranes manufactured using advanced sintering techniques demonstrate performance characteristics promising for the practical applications.

5. Acknowledgements

6. References

Annenkov, Yu. (1996). Physical foundations high-temperature electron-beam of ceramics, *Russian Physics Journal*, 39, No. 11, 1146-1159, ISSN: 1573-9228
Alexeff, I. & Meek, T. (2011). The effect of electric field intensity on the microwave sintering of zirconia, *Materials Letter*, 65, 2111-2113, ISSN: 0167-577X

Charmond, S.; Carry, C. & Bouvard, D. (2010). Densification and microstructure evolution of Y-tetragonal zirconia polycrystal powder during direct and hybrid microwave sintering in a single mode cavity, *Journal of European Ceramic Society*, 30, 1211-1221, ISSN: 0955-2219

Chiba, R.; Tabata, Y.; Komatsu. T.; Orui, H.; Nozawa, K.; Arakawa M. & Arai H. (2008). Property change of a $LaNi_{0.6}Fe_{0.4}O_3$ cathode in the initial current loading process and the influence of a ceria interlayer, *Solid State Ionics.*, 178, 1701-1705, ISSN: 0167-2738.

Cutler, R & Meixner D. (2003). Ceria–lanthanum strontium manganite composites for use in oxygen generation systems, *Solid State Ionics,* 159, 9-19, ISSN: 0167-2738.

Gil, V; Tartaj, J; Moure, C. & Duran P. (2007). Rapid densification by using Bi_2O_3 as an aid for sintering of gadolinia-doped ceria ceramics, *Ceramics International,* 33, 471-475, ISSN: 0272-8842.

Ivanov, V.; Khrustov, V; Kotov Yu, Medvedev, A.; Murzakaev, A.; Shkerin, S. & Nikonov, A. (2007). Conductivity and structure features of $Ce_{1-x}Gd_xO_{2-\delta}$ solid electrolytes fabricated by compaction and sintering of weakly agglomerated nanopowders, *Journal of the European Ceramic Society*, 27, 1041-1046, ISSN: 0955-2219.

Yamamoto, O. (2000) Solid oxide fuel cells: fundamental aspects and prospects *Electrochimica Acta*, 45, 2423-35, ISSN 0013-4686

Jiao, Z.; Shikazono, N. & Kasagi, N. (2011). An ultra-fast fabrication technique for anode support solid oxide fuel cells by microwave, *Journal of Power Sources*, 196, 5490-5493, ISSN: 0378-7753.

Jung, H.; Hong, K.-S.; Jung, H.-G.; Kim, H.; Kim, H.-R.; Son, Ji-W.; Kim, J.; Lee, H.-W. & Lee, J.-H. (2007). SOFCs with Sc-Doped Zirconia Electrolyte and Co-Containing Perovskite Cathodes, *Proceedings of the Electrochemical Society.*, 154, 480-485, ISSN: 1945-7111.

Kharlamova, T.; Pavlova, S.; Sadykov V., Bespalko, Y., Krieger, T.; Pelipenko, V.; Belyaev, V.; Muzykantov, V.; Alikina, G.; Okhlupin, Yu.; Uvarov, N. & Smirnova, A. (2011) Nanocomposite Cathode Materials for Intermediate Temperature Solid Oxide Fuel Cells, *ECS Transactions*, 35, 2331-2340, ISSN: 1938-5862

Kobayashi, K.; Takahashi, I.; Shiono, M. & Dokiya M. (2002). Supported $Zr(Sc)O_2$ SOFCs for reduced temperature prepared by electrophoretic deposition, *Solid State Ionics*, 152-153, 591-596, ISSN: 0167-2738.

Kumar,. S. (2003) Selective Laser Sintering:A Qualitative and Objective Approach *Journal of the Minerals,* 55, 43-47, ISSN 1047-4838

Laukaitis, G.; Dudonis, J. & Milčius D. (2007). Formation of Gadolinium Doped Ceria Oxide Thin Films by Electron Beam Deposition, *Materials Science (Medžiagotyra)*, 13, 23-26, ISSN: 1392-1320.

Lee, J.-S.; Choi, K.-H; Ryu, B.-K, Shin, B.-C. & Kim I.-S. (2004). Effects of alumina additions on sintering behavior of gadolinia-doped ceria, *Ceramics International*, 30, 807-812, ISSN: 0272-8842

Lee, J.-S.; Choi, K.-H; Ryu, B.-K, Shin, B.-C. & Kim I.-S. (2004). Effects of gallia additions on sintering behavior of gadolinia-doped ceria, *Materials Research Bulletin*, 39, 2025-2033, ISSN: 0025-5408.

Lemkey, F. & Movchan B. (2005). Synthesis of porous and dense elements of SOFC by electron beam physical vapor deposition (EBPVD), In: *Fuel Cell Technologies: State*

and Perspectives, Sammes, N et al. (Ed.), pp. 73-80, Springer, ISBN: 978-1-4020-3496-1, Netherlands.

Liu, Y.; Yin, C.; Wang, L; Li, D; Lian, J.; Hu, J. & Guo, Z. (2008). Properties of a Ceria-Based (C6S2G2) Solid Oxide Electrolyte Sintered with Al_2O_3 Additive, *Science of Sintering,* 40, 13-20, ISSN: 0350-820X

Ma, J.; Zhang, T.; Kong, L; Hing, P. & Chan, S. (2004). $Ce_{0.8}Gd_{0.2}O_{2-\delta}$ ceramics derived from commercial submicron-sized CeO_2 and Gd_2O_3 powders for use as electrolytes in solid oxide fuel cells, *Journal of Power Sources,* 132, 71-76, ISSN: 0378-7753.

Mazaheri, M.; Zahedi, A. & Hejazi, M. (2008). Processing of nanocrystalline 8 mol.% yttria-stabilized zirconia by conventional, microwave-assisted and two-step sintering, *Materials Science and Engineering: A*, 492, 261-267, ISSN: 0921-5093

Minh, N.Q. (1993). Ceramic Fuel Cells, *Ceram. Soc.,* 76, 563-588, ISSN: 0002-7820.

Pérez-Coll, D.; Núñez, P.; Frade, J. & Abrantes C. (2003). Conductivity of CGO and CSO ceramics obtained from freeze-dried precursors, *Electrochimica Acta,* 48, 1551-1557, ISSN: 0013-4686

Sadykov, V.; Kharlamova, T.; Batuev, L.; Mezentseva, N.; Alikina, G.; Muzykantov, V.; Krieger, T.; Pavlova, S.; Zaikovskii, V.; Ishchenko, A.; Zarubina, V.; Rogov, V.; Bobrenok, O.; Uvarov, N.; Kilner, J.; Druce, J. & Smirnova, A. (2008). Design and Characterization of Nanocomposites Based on Complex Perovskites and Doped Ceria as Advanced Materials for Solid Oxide Fuel Cell Cathodes and Membranes, *Mater. Res. Soc. Symp. Proc.*, 1098, 1-6, ISSN: 0272-9172.

Sadykov, V.; Muzykantov, V.; Bobin, A.; Batuev, L.; Alikina, G.; Lukashevich, A.; Boronin, A.; Krieger, T.; Ishchenko, A.; Bobrenok, O.; Uvarov, N.; Smirnova, A. & Vasylyev, O. (2009). Design and characterization of LSM-ScCeSZ nanocomposite as MIEC material for SOFC cathodes and oxygen-separation membranes., *Mater. Res. Soc. Symp. Proc.*, 1126, 1-6, ISSN: 0272-9172.

Sadykov, V.; Pavlova, S.; Zarubina ,V.; Bobin, A.; Alikina, G.; Lukashevich, A.; Muzykantov, V.; Usoltsev, V.; Kharlamova, T.; Boronin, A.; Koscheev, S.; Krieger, T.; Ishchenko, A.; Mezentseva, N.; Salanov, A.; Smirnova, A.; Bobrenok, O. & Uvarov, N. (2009). Design and Characterization of Functionally Graded Cathode Materials for Solid Oxide Fuel Cells, *ECS Trans.*, 25, 2403-2412, ISSN: 1938-6737.

Sadykov, V.; Zarubina, V.; Pavlova, S. et al. (2010). Design of asymmetric multilayer membranes based on mixed ionic–electronic conducting composites supported on Ni–Al foam substrate, *Catalysis Today,* No. 156, (October 2010) pp. 173-180, ISSN: 0920-5861

Sadykov, V.; Pavlova, S.; Kharlamova, T.; Muzykantov, V.; Uvarov, N.; Okhlupin, Yu.; Ishchenko, A.; Bobin, A.; Mezentseva, N.; Alikina G., Lukashevich, A.; Krieger, T.; Larina, T.; Bulgakov, N.; Tapilin, V.; Belyaev, V.; Sadovskaya, E.; Boronin, A.; Sobyanin, V.; Bobrenok, O.; Smirnova, A.; Smorygo O. & Kilner J. (2010) Perovskites and Their Nanocomposites with Fluorite-Like Oxides as Materials for Solid Oxide Fuel Cells Cathodes and Oxygen-Conducting Membranes, In: *Perovskites: Structure, Properties and Uses,* Borowski, M (Ed.), pp. 67-178, Nova Science Publishers, Inc. New York, ISBN: 978-1-61668-525-6, .

Sadykov, V; Mezentseva, N.; Usoltsev, V., Sadovskaya , E., Ishchenko, A., Pavlova, S., Bespalko, Y., Kharlamova, T., Zevak, E., Salanov, A., Krieger, T., Belyaev, V., Bobrenok, O., Uvarov, N., Okhlupin, Yu., Smorygo, O., Smirnova, A.; Singh, P.,

Vlasov, A., Korobeynikov, M., Bryazgin. A., Kalinin, P. & Arzhannikov, A. (2011). Solid oxide fuel cell composite cathodes based on perovskite and fluorite structures, *Journal of Power Sources,* 196, 7104-7109, ISSN: 0378-7753.

Sadykov, V., Usoltsev, V., Fedorova, Yu., Sobyanin, V., Kalinin, P., Arzhannikov, A., Vlasov, A., Korobeynikov, M., Bryazgin; A., Salanov, A., Predtechenskii, M., Bobrenok, O., Ulikhin, A., Uvarov, N., Smorygo, O., Il'yushchenko, A., Ul'yanitskii, V., Zlobin, S. (2011). Design of medium–temperature solid oxide fuel cells on porous supports of deformation strengthened Ni–Al alloy. *Russian Journal of Electrochemistry*, 47, 488–493. ISSN: 1023-1935.

Schiller, G.; Henne, R; Lang, M.; Ruckdaschel, R. & Schaper, S. (2000) Development of vacuum plasma sprayed thin-film SOFC for reduced operating temperature, *Fuel Cells Bulletin*, pp. 7-12, ISSN: 1464-2859.

Singh, J. & Wolfe D. (2005). Nano and macro-structured component fabrication by electron beam-physical vapor deposition (EB-PVD), *Journal Of Materials Science,* 401-26, ISSN: 1573-4803.

Smorygo, O.; Mikutski, V.; Leonov, A.; Marukovich, A. & Vialiuha, Y. (2008) Nickel foams with oxidation-resistant coatings formed by combustion synthesis, *Scripta Materialia,* 58, 910-913, ISSN: 1359- 6454.

de Souza, S.; Visco, S. & de Jonghe, L. (1997). Thin-film solid oxide fuel cell with high performance at low-temperature, *Solid State Ionics.*, 98, 57-60, ISSN: 0167-2738.

Tucker, M. (2010). Progress in metal-supported solid oxide fuel cells: A review, *J. Power Sources*, 195, 4570-4582, ISSN: 0378-7753.

Yamane H. & Hirai T. (1987). Preparation of ZrO_2-film by oxidation of $ZrCl_4$, *Materials Science Letters*, 6, 1229-1235, ISSN: 0261-8028.

Zaeh, M. & Kahnert, M. (2009). The effect of scanning strategies on electron beam sintering, *Prod. Eng. Res. Devel.*, 3, 217-224, ISSN: 0022-1817.

Zhang, T. & Ma, J. (2004). Dense submicron-grained $Ce_{0.8}Gd_{0.2}O_{2-d}$ ceramics for SOFC applications, *Scripta Materialia*, 50, 1127-1130, ISSN: 1359- 6454.

Zhang, T; Ma, J; Kong, L; Chan, S; Hing, P. & Kilner J. (2004). Iron oxide as an effective sintering aid and a grain boundary scavenger for ceria-based electrolytes, *Solid State Ionics,* 167, 203-207, ISSN: 0167-2738
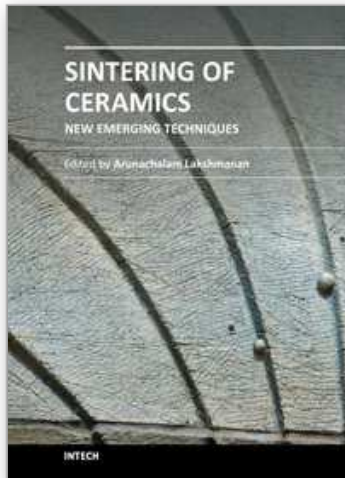
Sintering of Ceramics - New Emerging Techniques

Edited by Dr. Arunachalam Lakshmanan

The chapters covered in this book include emerging new techniques on sintering. Major experts in this field contributed to this book and presented their research. Topics covered in this publication include Spark plasma sintering, Magnetic Pulsed compaction, Low Temperature Co-fired Ceramic technology for the preparation of 3-dimesinal circuits, Microwave sintering of thermistor ceramics, Synthesis of Bio-compatible ceramics, Sintering of Rare Earth Doped Bismuth Titanate Ceramics prepared by Soft Combustion, nanostructured ceramics, alternative solid-state reaction routes yielding densified bulk ceramics and nanopowders, Sintering of intermetallic superconductors such as MgB2, impurity doping in luminescence phosphors synthesized using soft techniques, etc. Other advanced sintering techniques such as radiation thermal sintering for the manufacture of thin film solid oxide fuel cells are also described.

How to reference

In order to correctly reference this scholarly work, feel free to copy and paste the following:

INTECH

open science | open minds